Investigation of porous microstructure of plasma-sprayed coatings

Pavel Ctibor, Viktor Beneš, Radka Lechnerová

Institute of Plasma Physics, Academy of Sciences of the Czech Republic,
Department of Probability and Mathematical Statistics, Faculty of Mathematics and Physics,
Charles University in Prague, Czech Republic

MIPOM Workshop, Université Paris Descartes,
January 12–16, 2009

Thermally sprayed coatings

Use: Protection of surfaces, thermal barrier

Quantification and visualization of coating microstructure:

a) better insight in the microstructure: semi-globular pores, interlamellar flat pores

b) distinction between coatings sprayed by different techniques and with variety of process parameters

c) relation between the geometry of pores and physical properties of coatings

Two parts of the talk:

(i) use of stochastic geometry for the quantification

(ii) visualization results

Getting information

Condition for visualization: segmentation of microscopic images

3D information from serial sections

light or scanning electron microscopy

image analysis

Other approaches: x-ray computerized microtomography (CMT), (Kulkarni et al. 2000)

x-ray scattering (USAXS) technique, (Kulkarni et al. 2005)

small angle neutron scattering (SANS), (Ilavsky et al. 1998)

Computer-aided volumetric representation

a) Volumetric reconstruction

grinding, polishing, serial sections,

image analysis, software Lucia

3D computer reconstruction

b) Volumetric description

estimation of statistical and stereological characteristics in 3D

modelling of the porous microstructure

c) Volumetric visualization

rendering of reconstructed images

perspective figures, animations, anaglyphs

software Voxblast, Amira, Voxler

Enamel coatings - surface protection

production: firing of the melt on a substrate

microstructure with spherical pores (bubbles)

estimation of the bubble density and size distribution

classical stereological approach: a single section

Wicksell corpuscule problem, Saltykov histogram method

Volenik et al (1990), Silikaty - Ceramics.

Material

(i) plasma-sprayed coating based on ceramics

Titanates $MgTiO_3$, $CaTiO_3$, mixture with ratio $Mg : Ca = 94 : 6$

sample manufactored by water-stabilized plasma spray gun

in the Institute of Plasma Physics ASCR

feedstock powder size 63–125 μm

final coating thickness 1 mm

principal structural units - lamellas (splats)

result from spreading and solidification of droplets

3D specimen investigated

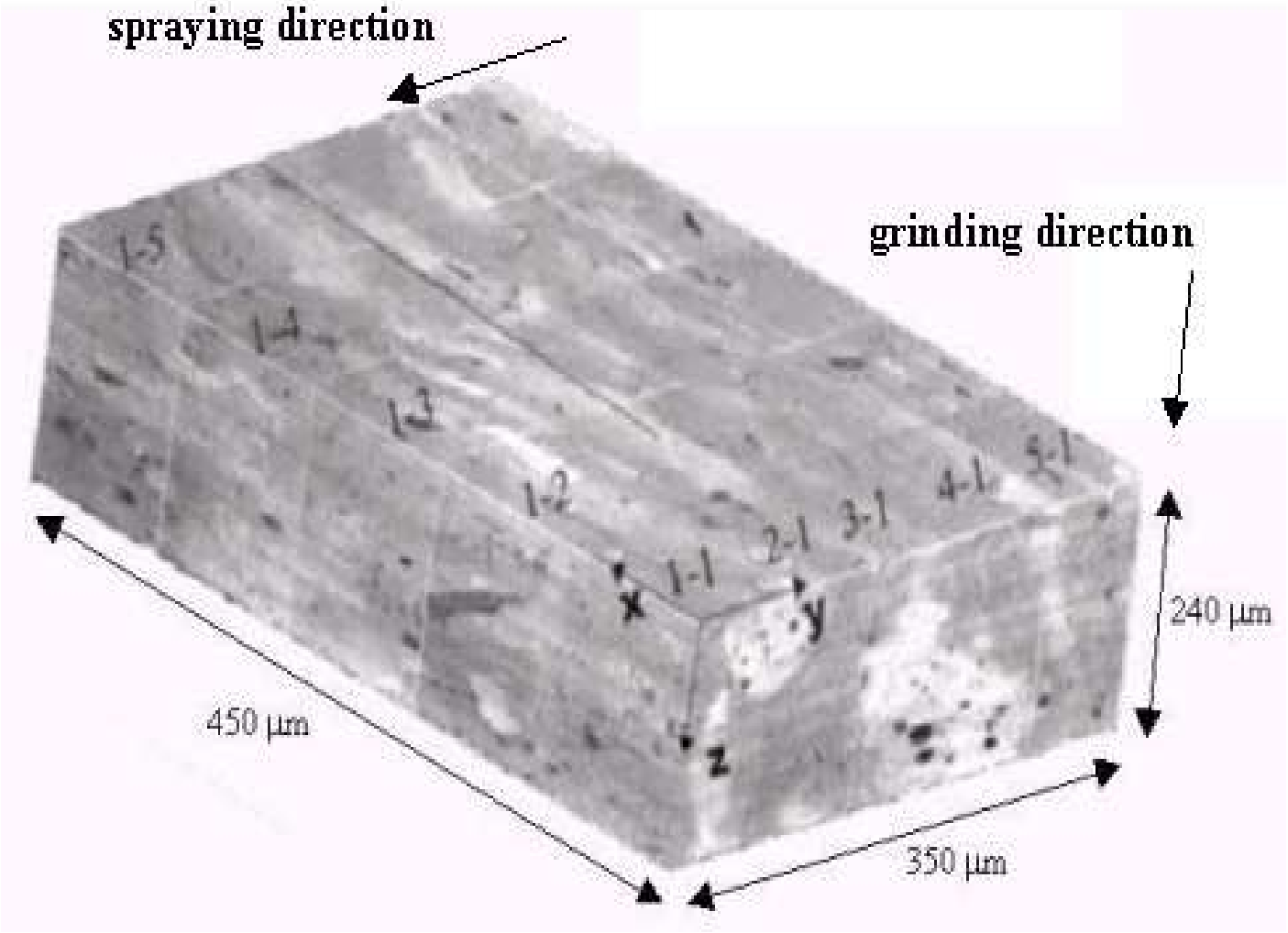

Figure: 80 serial sections obtained by light microscopy with subsequent grinding and polishing, distant 3 μm, on each section 5×5 images

Image analysis of a section

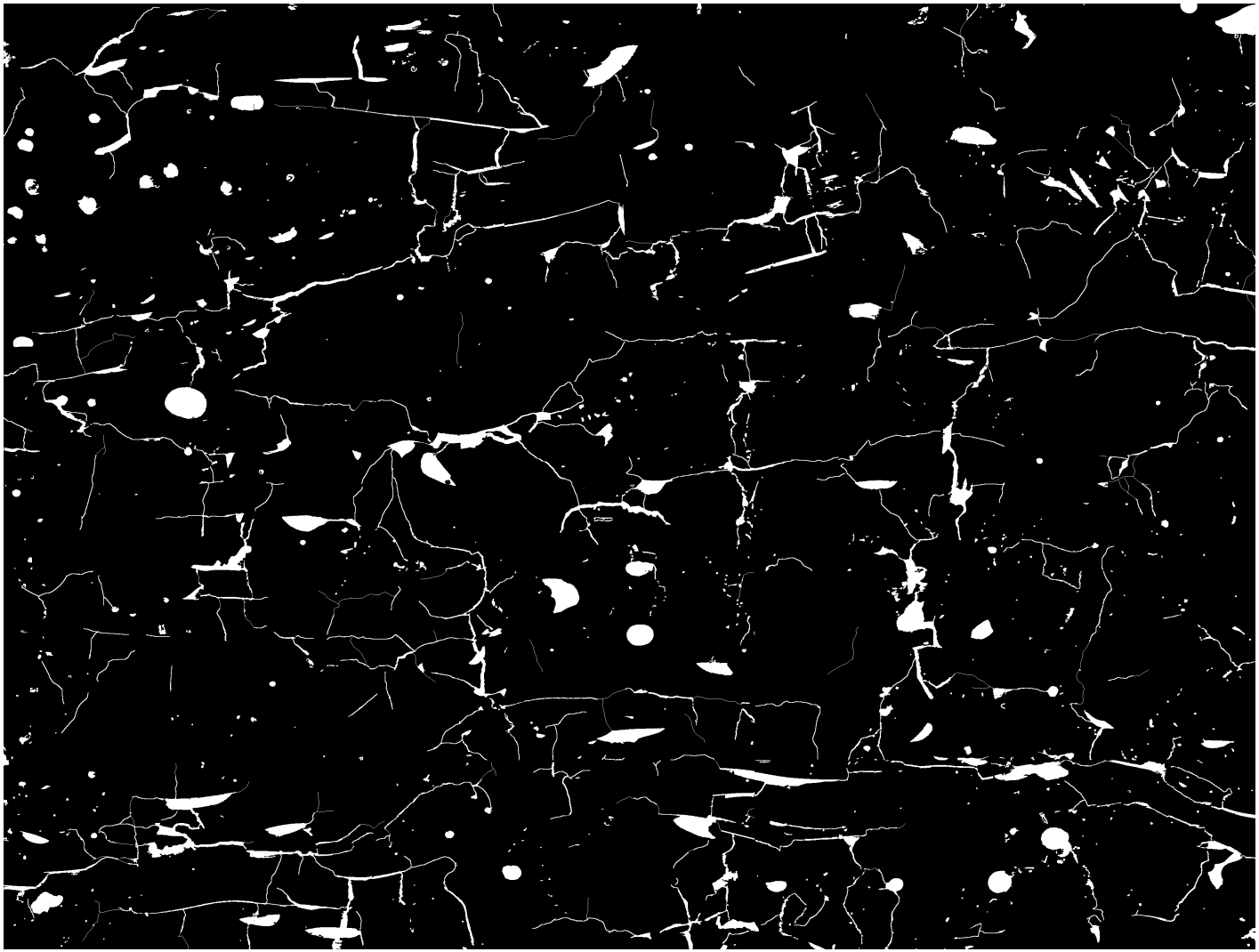

Figure: A montage of 5×5 images of a section after segmentations w.r.t. pores (white)

Classification of pores

a) semi-globular pores - almost convex, result from imperfect adhesion.

Detected by morphological opening, convex structural element.

b) interlamellar flat pores - along the splats,

approximately perpendicular to the spraying direction;

after subtraction of semi-globular pores detected by opening with

linear structural element within range of suitable orientations

c) other cracks (not investigated here)

Semi-globular pores

Figure: Representation of a section of the plasma-sprayed coating with semi-globular pores (white)

3D reconstruction of semi-globular pores

2116 semi-globular pores observed (edge-correction)

2D parameters measured by image analyser: section centroid, area, minimal and maximal diameter (shape)

3D parameters reconstructed: pore centroid, volume (Cavalieri principle)

Size distribution of globular pores

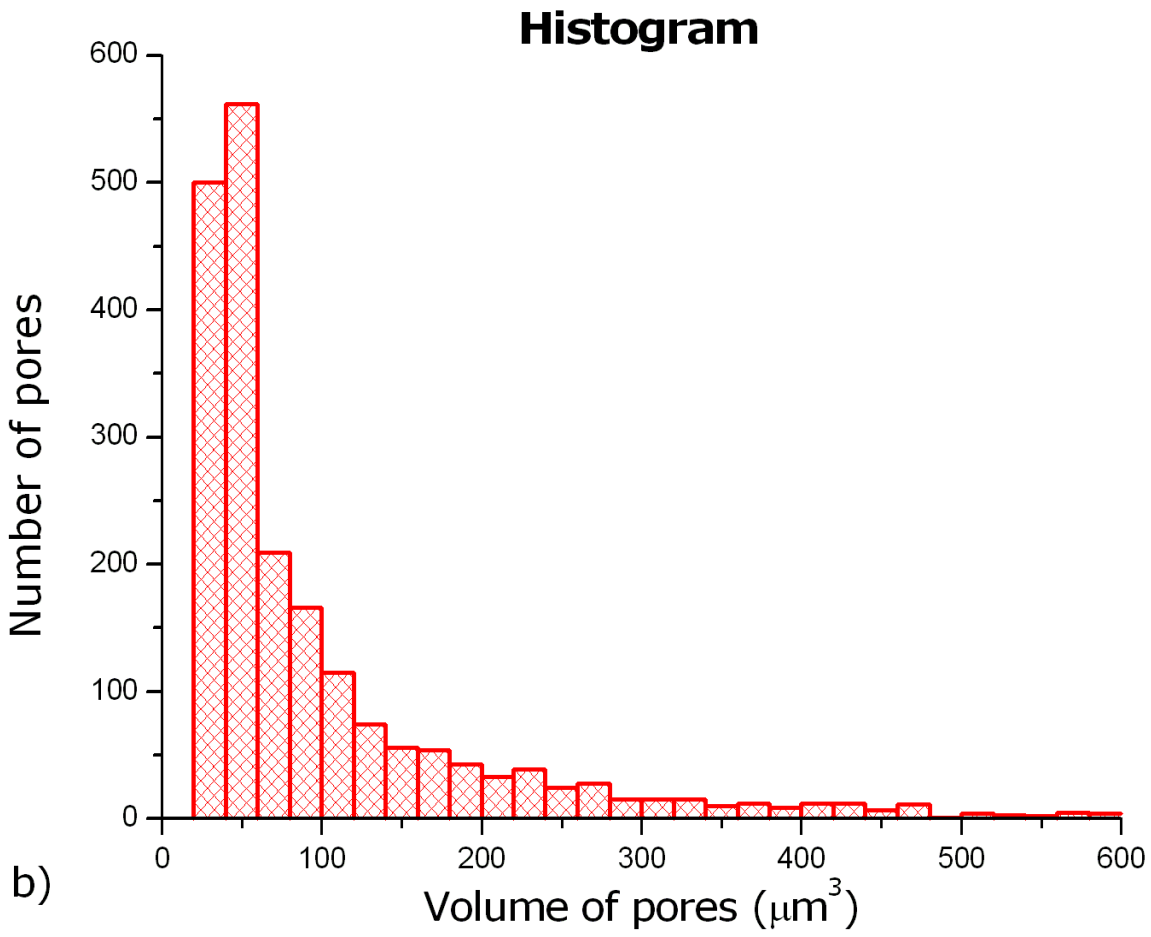

Figure: Histogram of estimated volumes [μm^3] of semi-globular pores, pores with diameters smaller than the distance between sections are not registered

Spatial distribution of semi-globular pores

Tests of complete spatial randomness based on centroids

a) L-function (second-order characteristics)

b) nearest neighbour distribution function

(edge correction)

95% confidence bounds

Complete randomness rejected, mild clustering

Test based on L-function

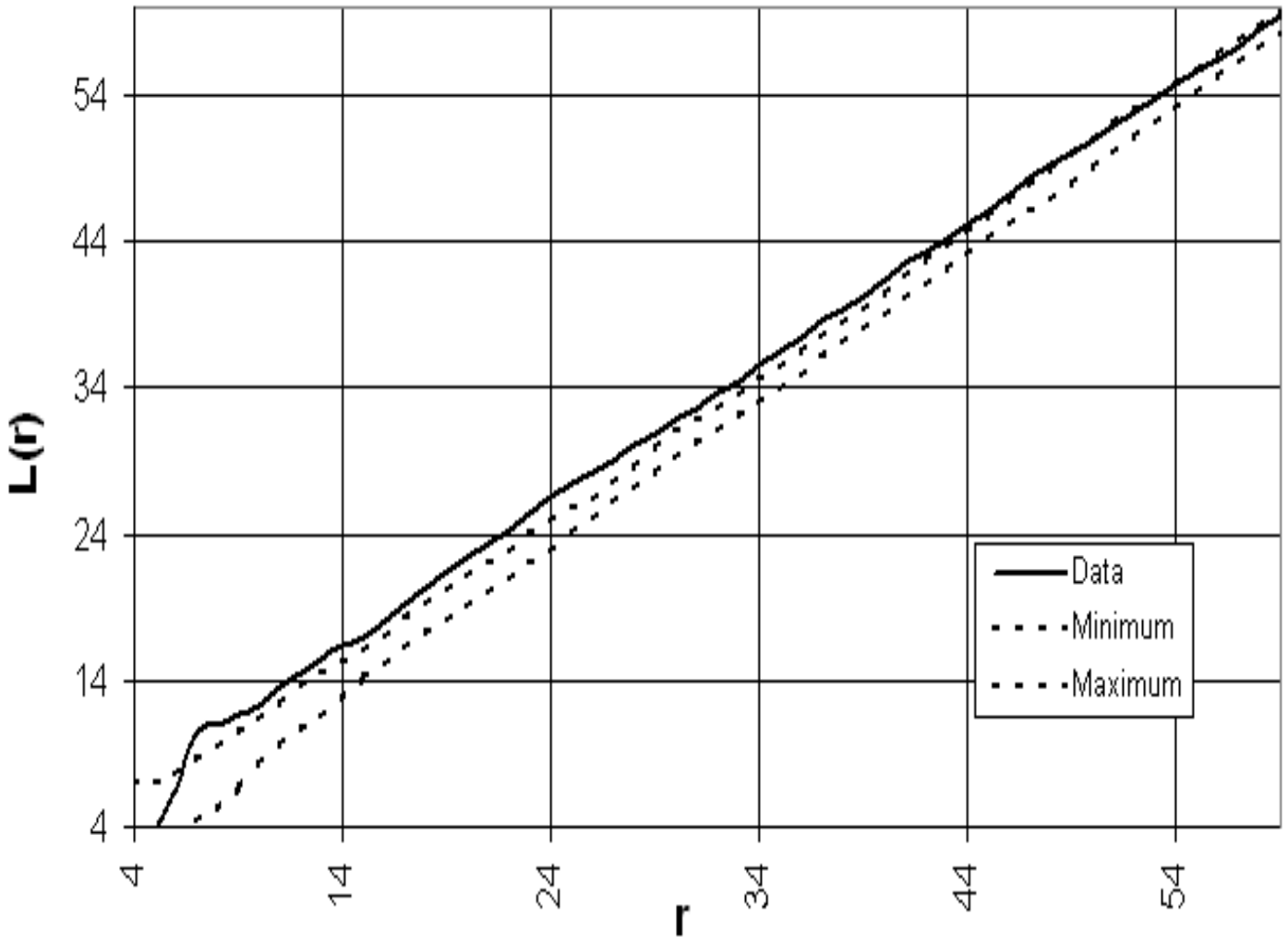

Figure: Graph of L-function is above 95% bounds for complete randomness which results in mild clustering

Test based on the nearest-neighbour distribution function

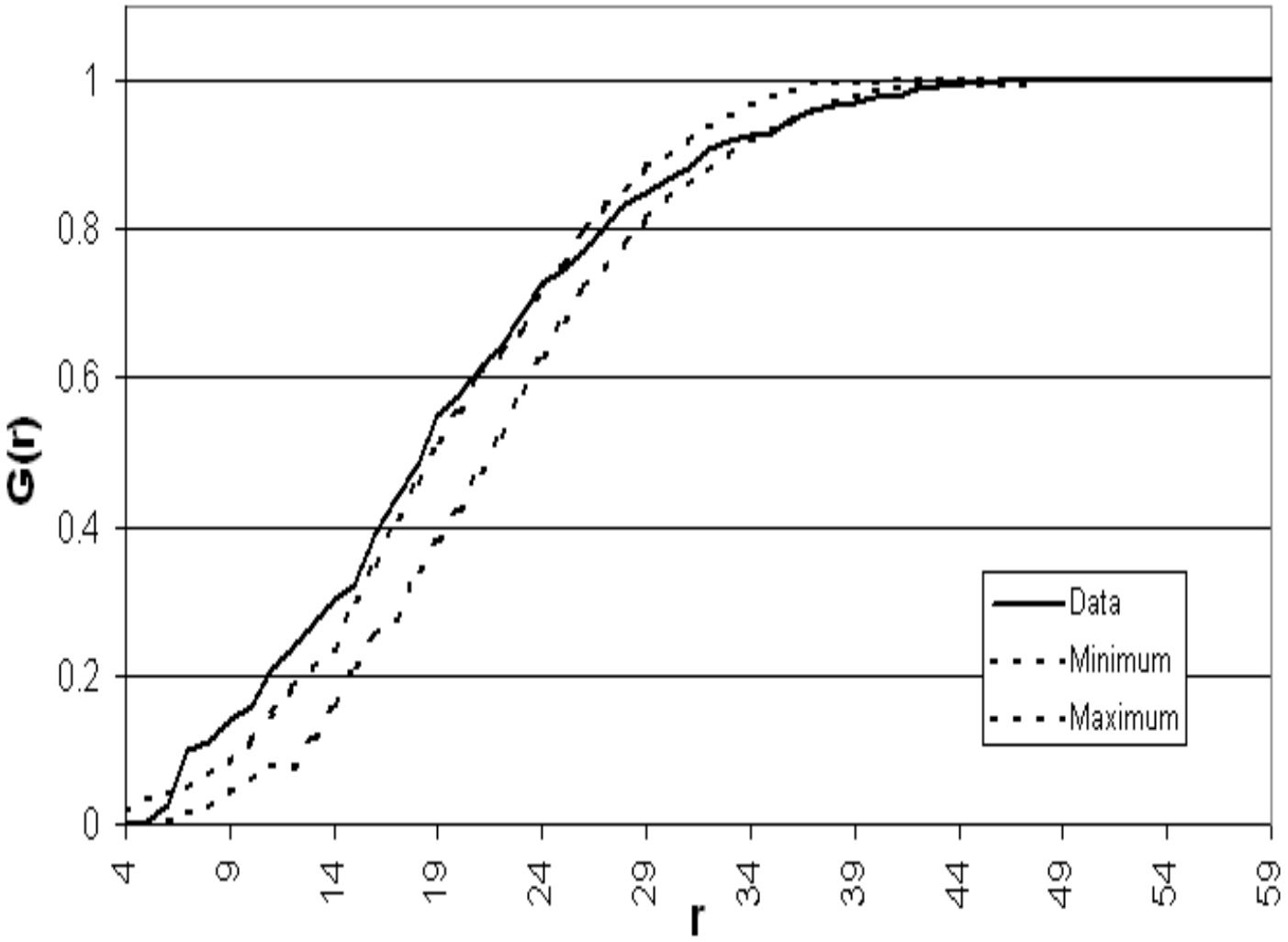

Figure: Graph of the nearest-neighbour distribution function is on small distances to the left of 95% bounds, complete spatial randomness is rejected

Interlamellar flat pores (IFP)

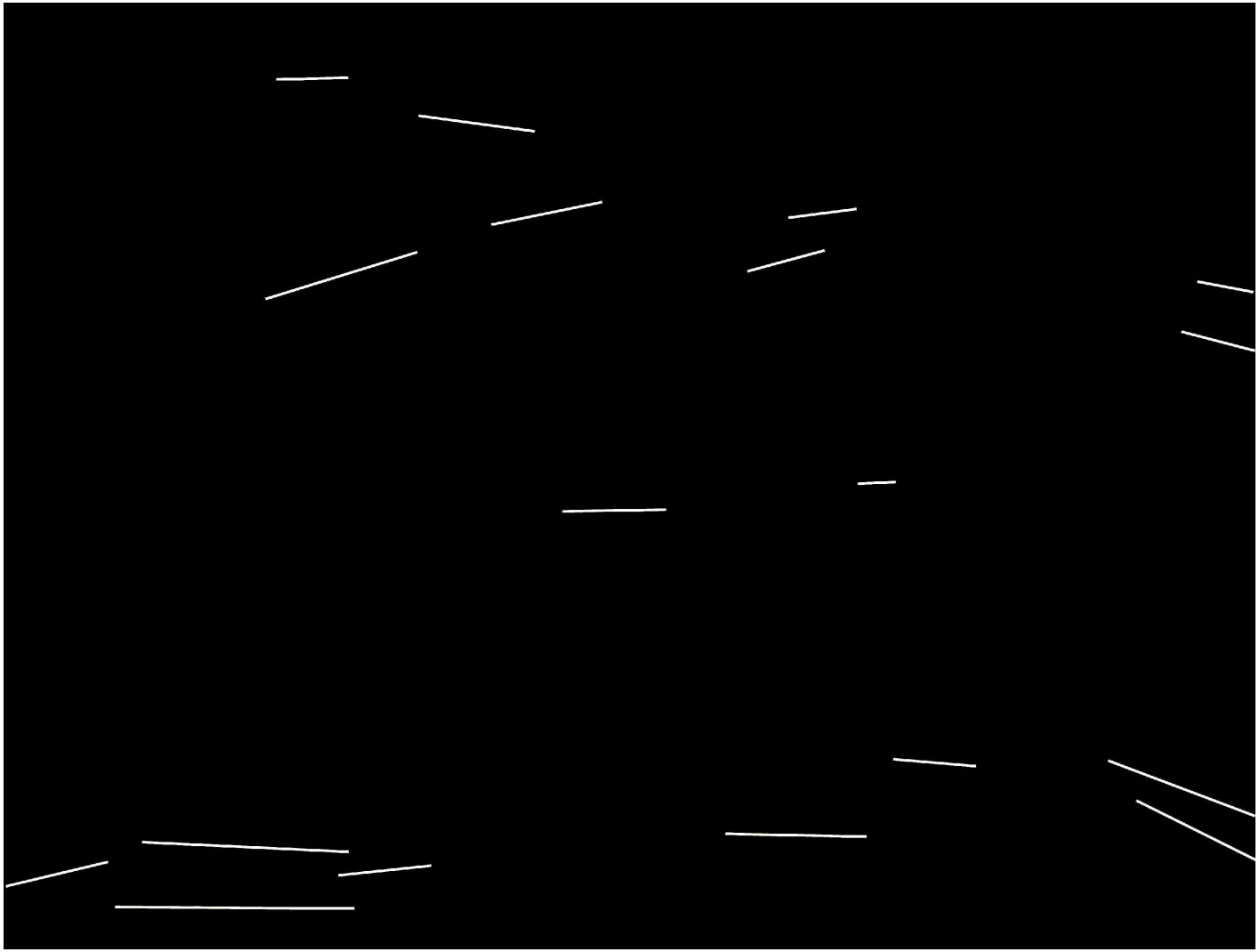

Figure: Sections of IFP approximated by segments

3D reconstruction of interlamellar flat pores

Zero thickness assumed

602 pores detected in more than one section

Triangulation enables estimation of surface area

Shape of intelamellar flat pores

Homogeneity of IFP along the spraying direction

Interlamellar flat pores

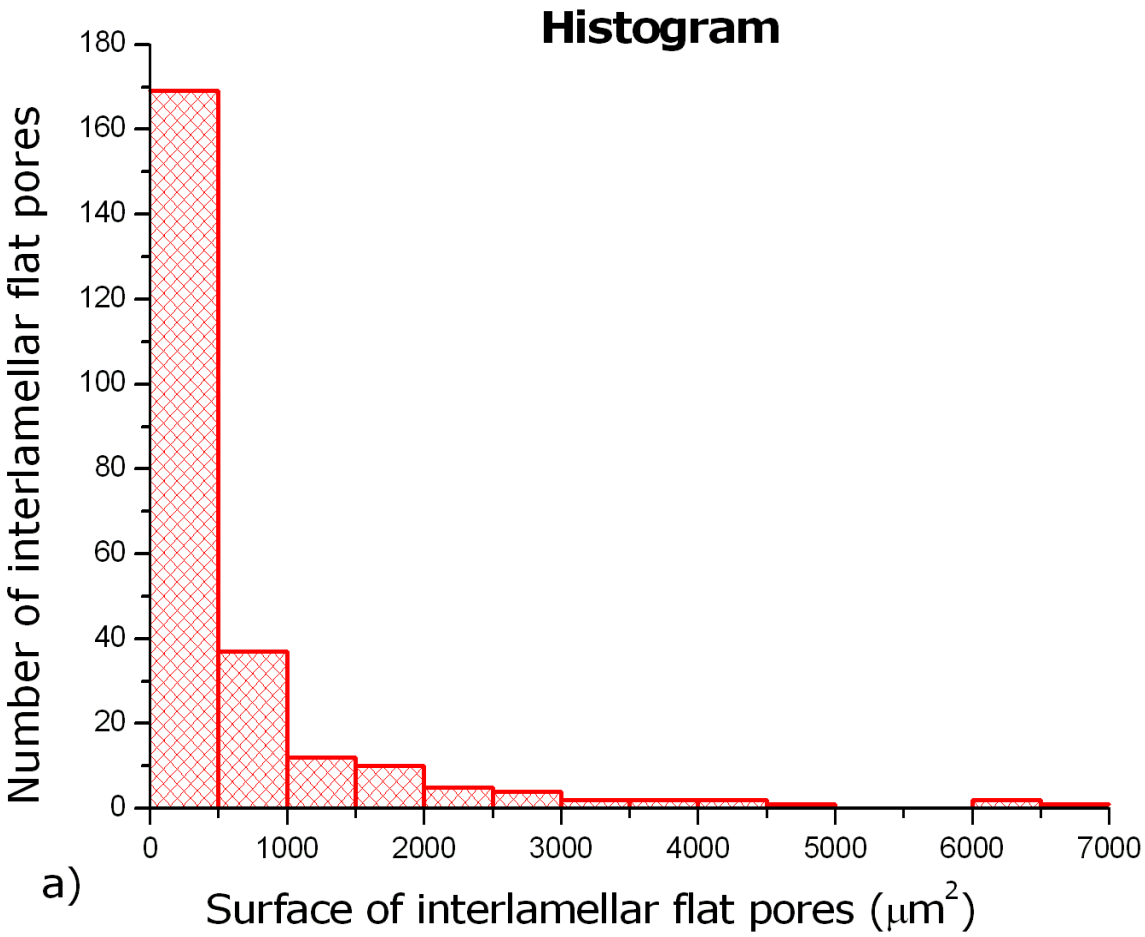

Figure: Histogram of surface areas [μm^2] of IFP

Interlamellar flat pores

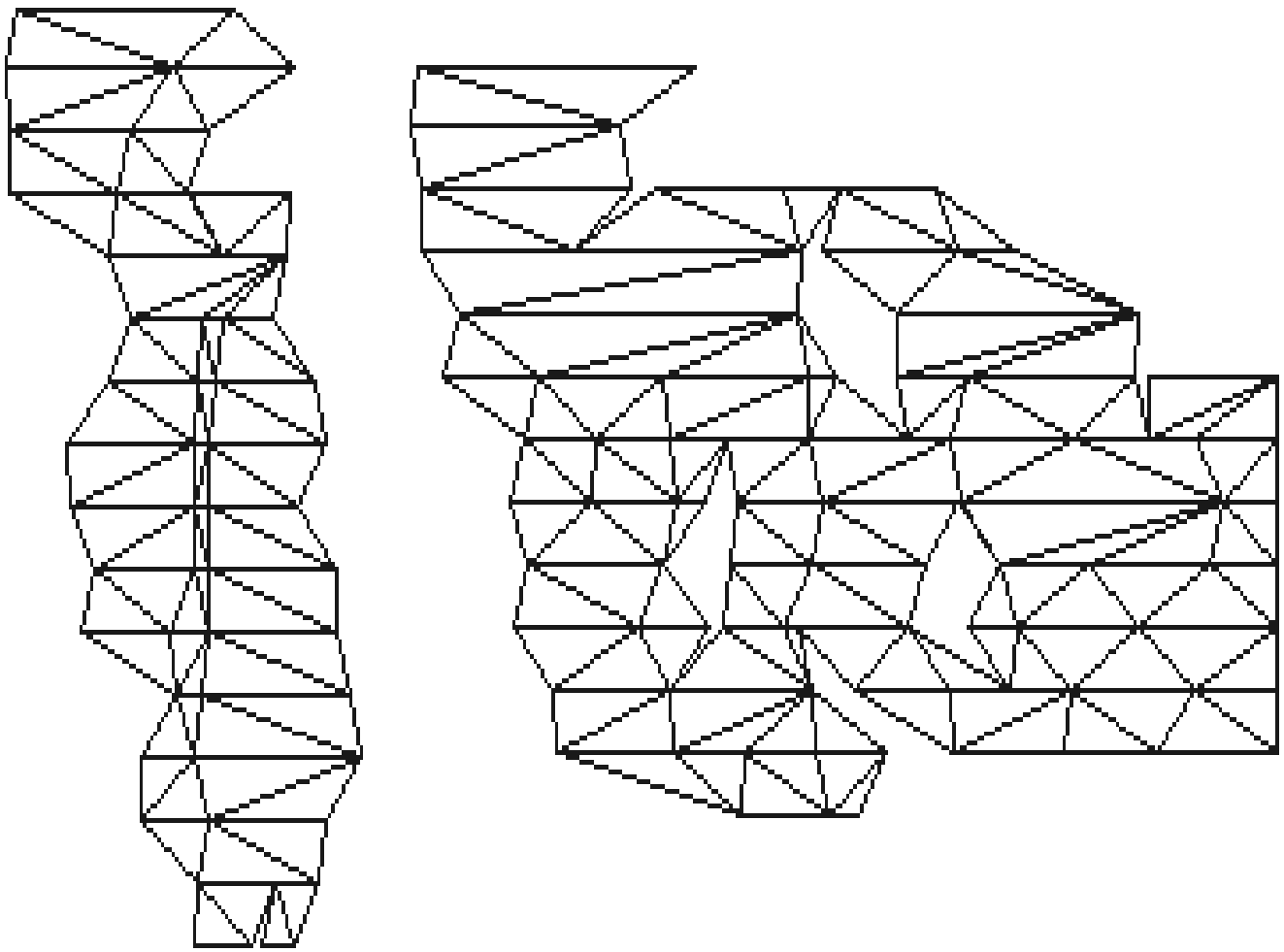

Figure: Shapes of largest individual IFP projected onto the plane perpendicular to the spraying direction

Homogeneity of IFP

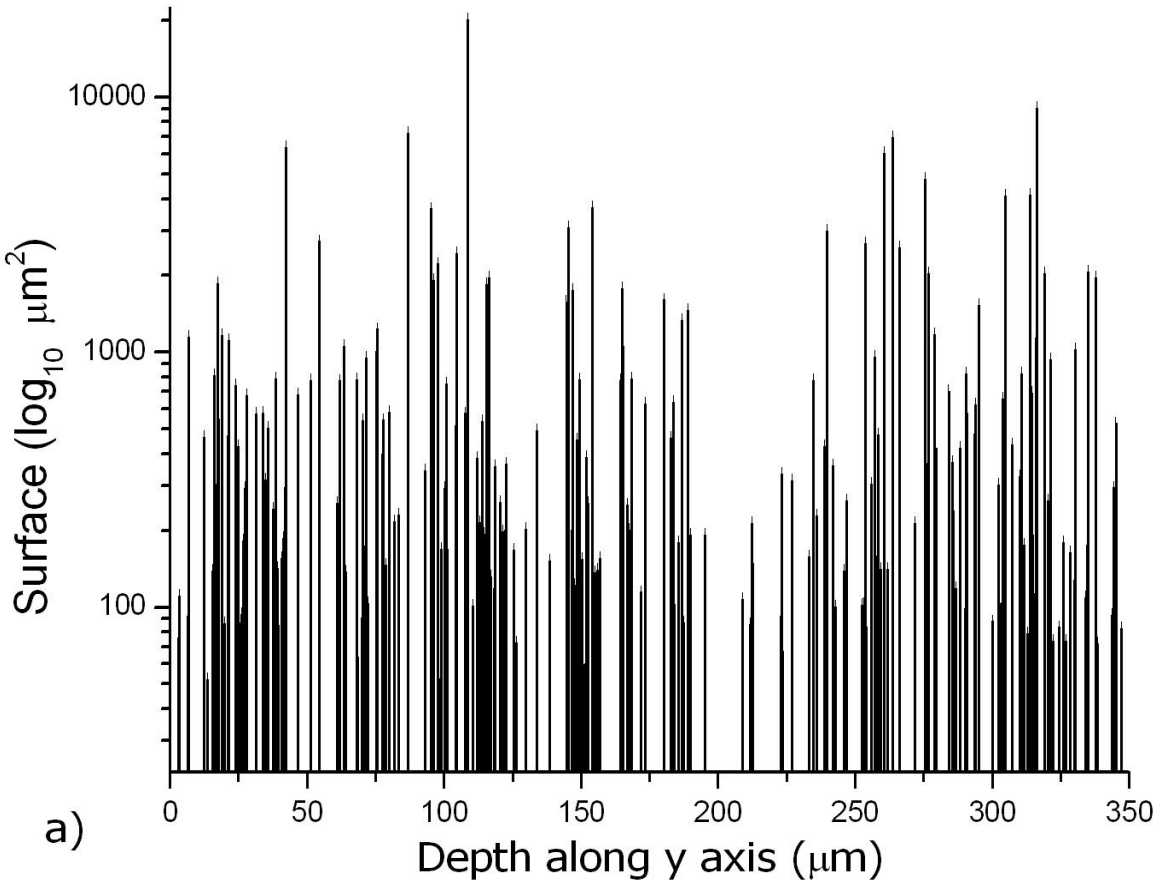

Figure: Surface areas [μm^2] of IFP along y-axis (spraying direction)

Homogeneity of IFP

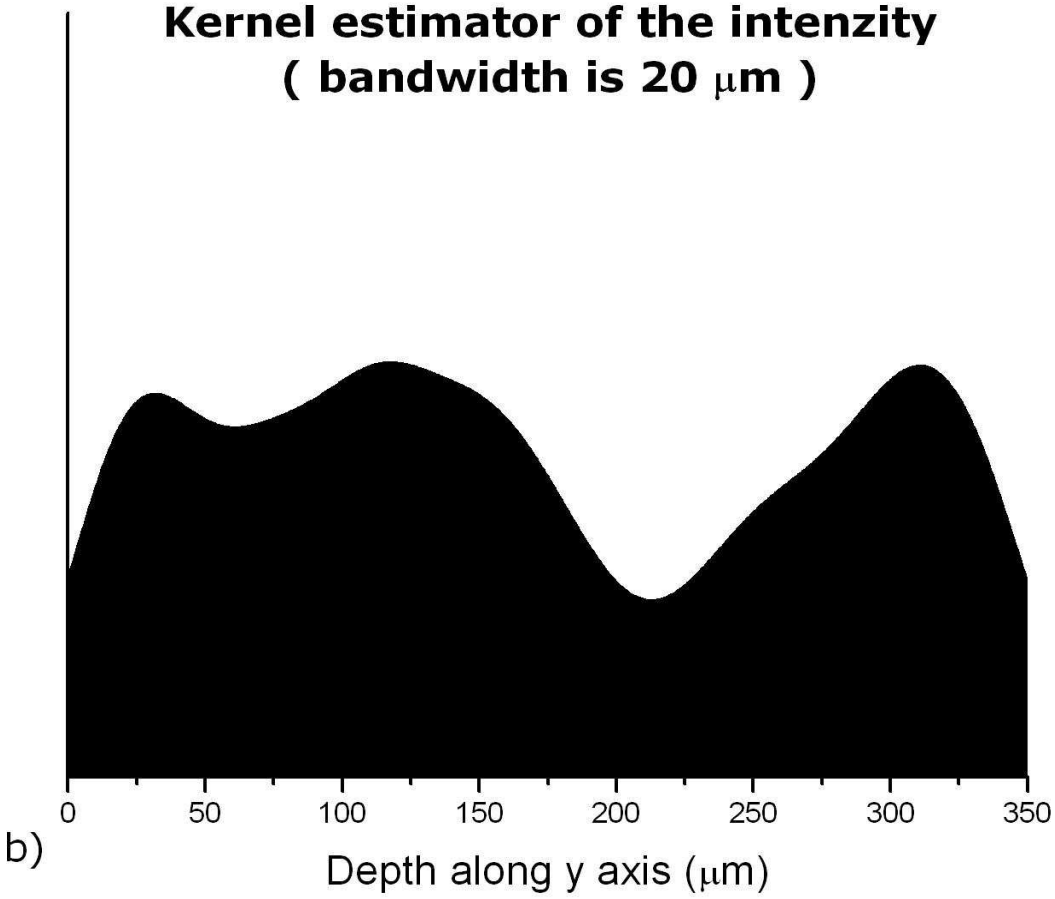

Figure: Kernel density estimator of the number of IFP along y-axis. The size (surface area) is not considered here.

Relationships between IFP and semi-globular pores

Mixed characteristics of both types of pores

a) comparison of nearest-neighbour distribution function for surfaces of semi-globular pores with distribution function of distances from semi-globular pores to the nearest IFP.

b) correlation field between the size of semi-globular pores and the location of the nearest IFP on y-axis.
Results in an overall homogeneity.

Joint characteristics of IFP and semi-globular pores

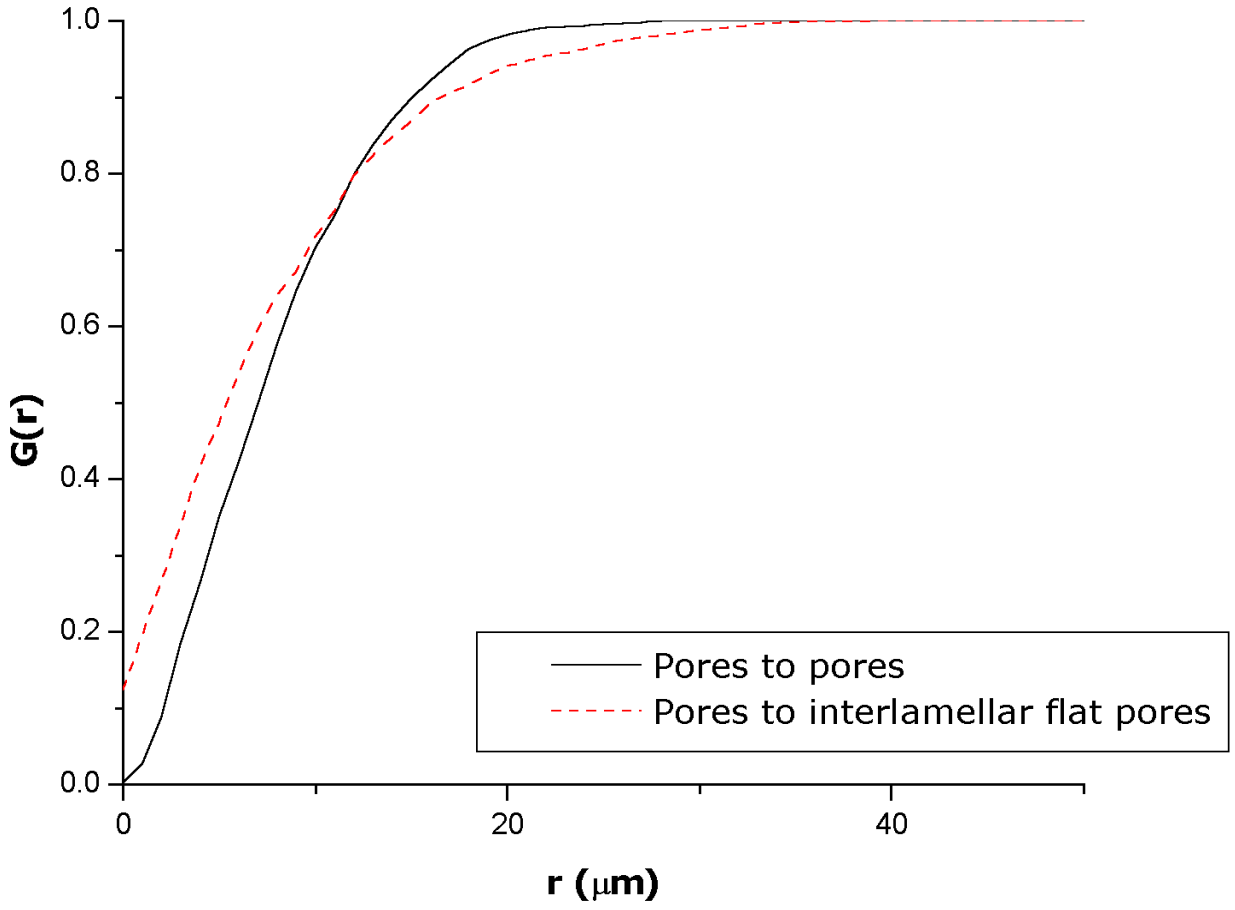

Figure: Nearest neighbour distribution functions of two types.

Joint characteristics of IFP and semi-globular pores

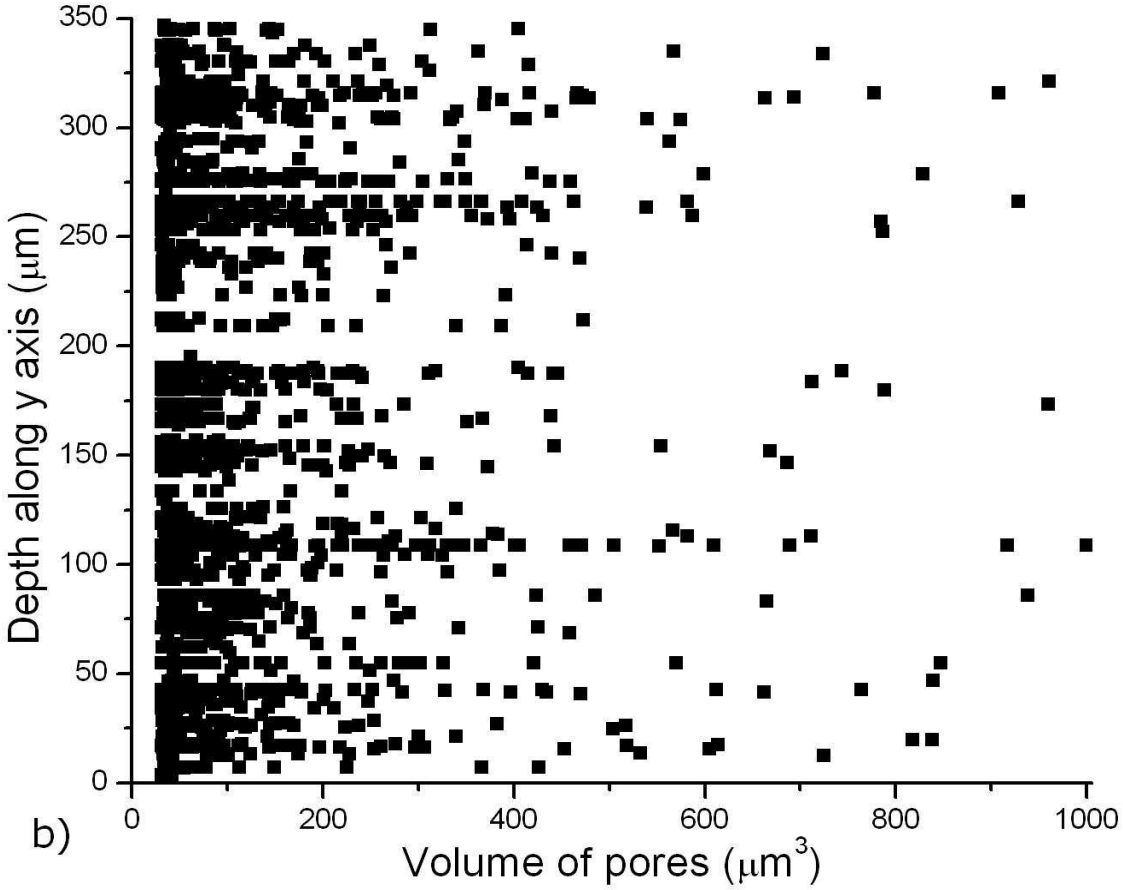

Figure: Correlation plot for the size of semi-globular pores and their location w.r.t. IFP

(ii) Comparison of different spraying techniques.

Quantitative description of the microstructure of coatings developed in part (i) used

Material: stainless steel AISI 316L

a) Wire-arc spraying performed at Škoda Research LtD, Plzeň, TAFA 9000 (USA) spray system

b) Water stabilized plasma-sprayed system WSP 500 (Institute of Plasma Physics, ASCR)

Main structural features: Porosity, oxide phase

Plasma sprayed coating, 3D specimen investigated

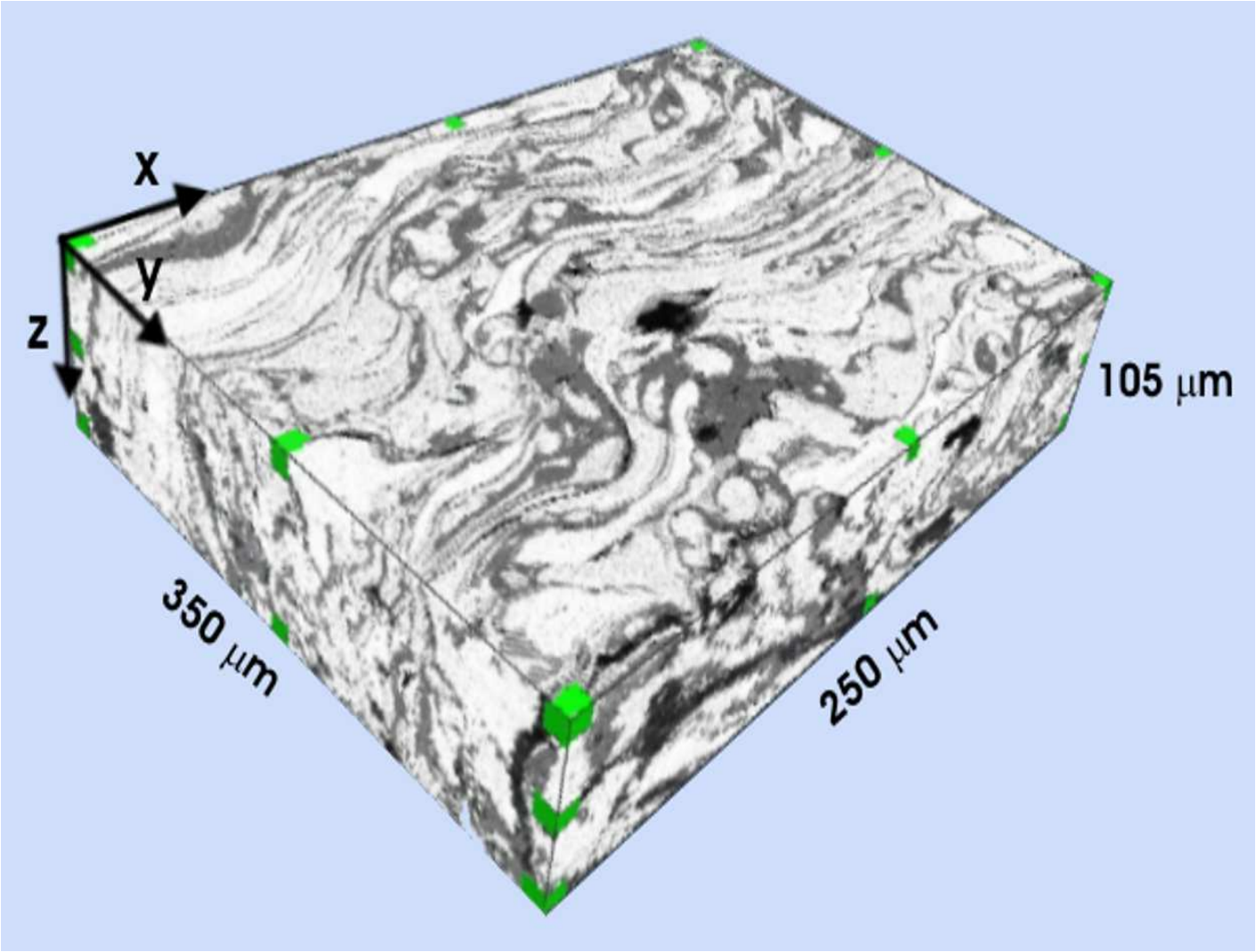

Figure: Pores black, oxides grey, basic matrix white. Spraying direction y-axis, grinding direction z-axis, 35 sections obtained distant about 5μm

Microstrucure of pores in a specimen section

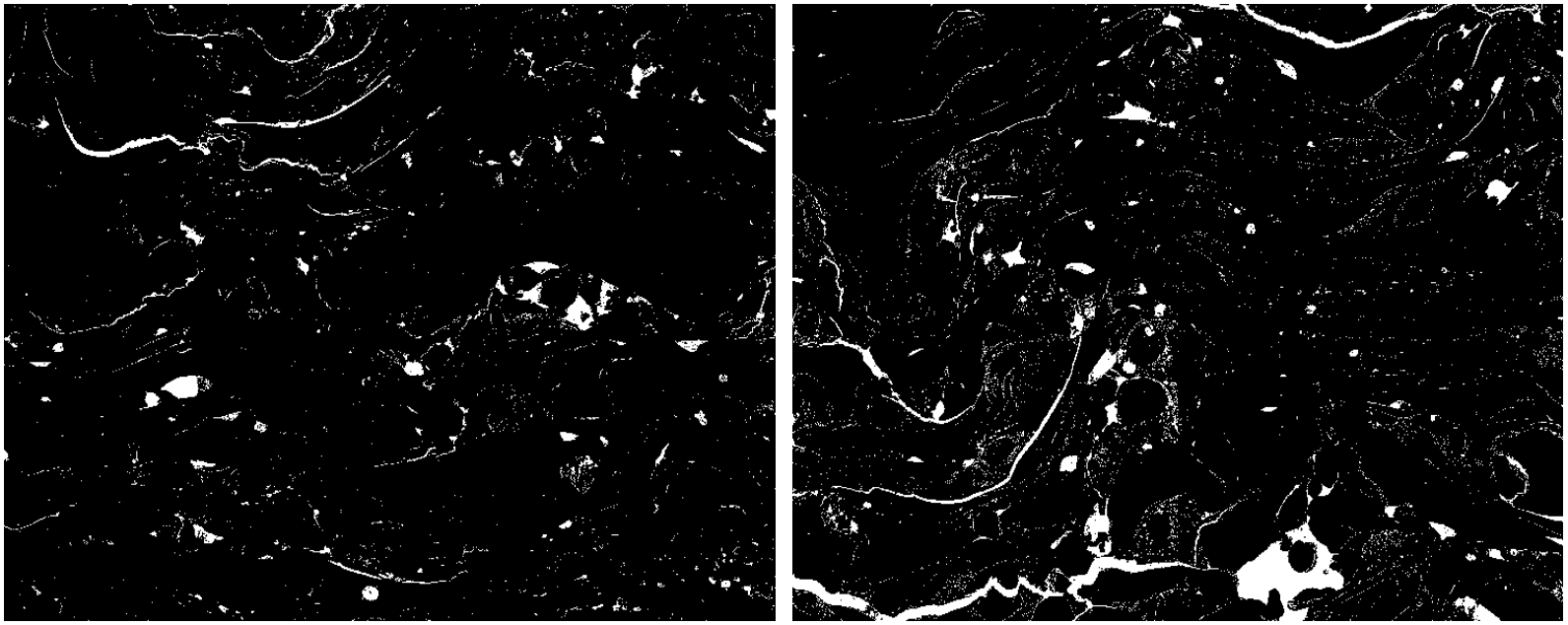

Figure: Wire-arc sprayed coating (left), plasma-sprayed coating (right), pores white

Microstrucure of oxides in a specimen section

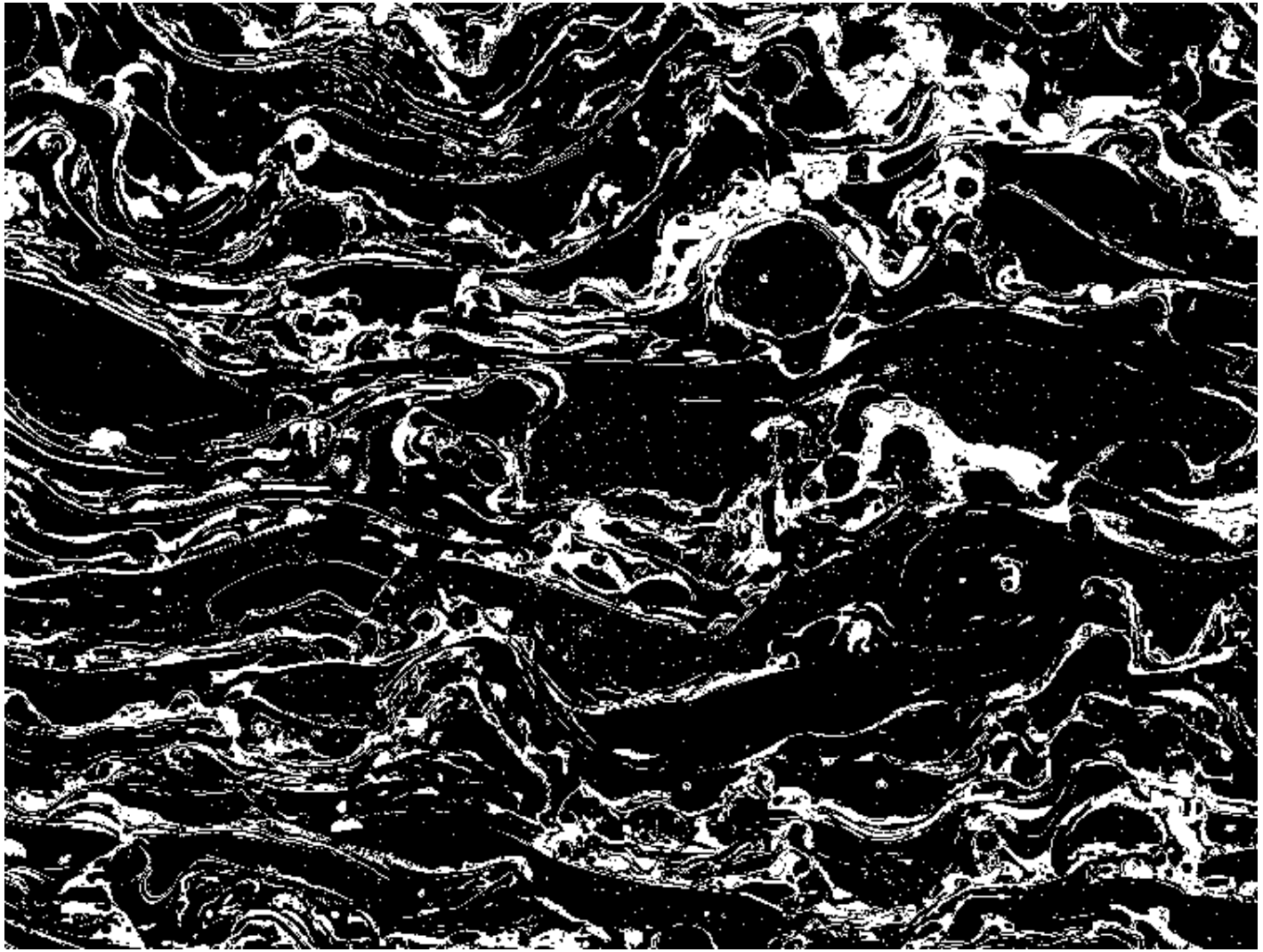

Figure: Wire-arc sprayed coating, oxides white

Quantification of pores in AS (wire-arc sprayed) and PS (plasma sprayed) coating

Maximum pore volume AS: 6602 μm^3, PS: 26016 μm^3

Number of pores (volume greater than 16 μm^3) AS: 814, PS: 879

Volume fraction of pores AS: 0.82%, PS: 1.92%

Volume fraction of oxides AS: 23%, PS: 30%

Size distributions of pores

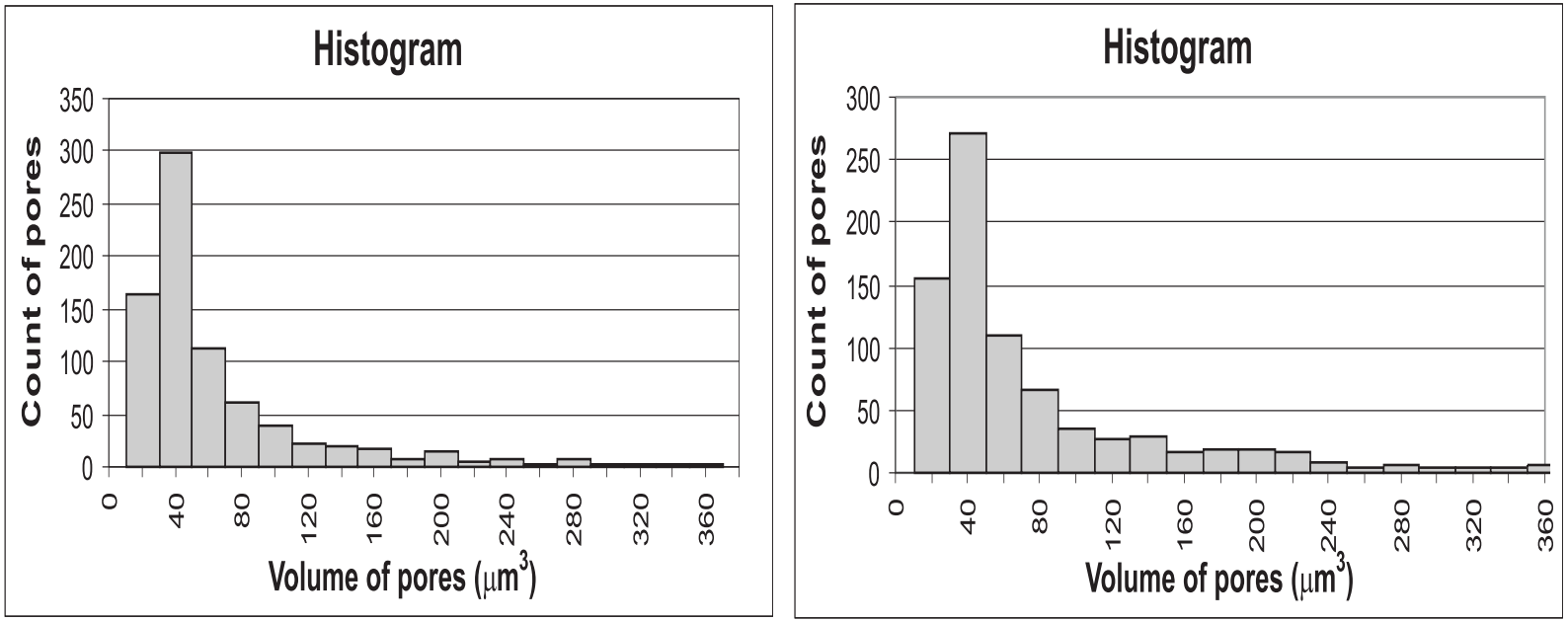

Figure: Wire-arc sprayed coating (left), plasma-sprayed coating (right), histograms of volume of pores

Area fraction of oxides along the section planes

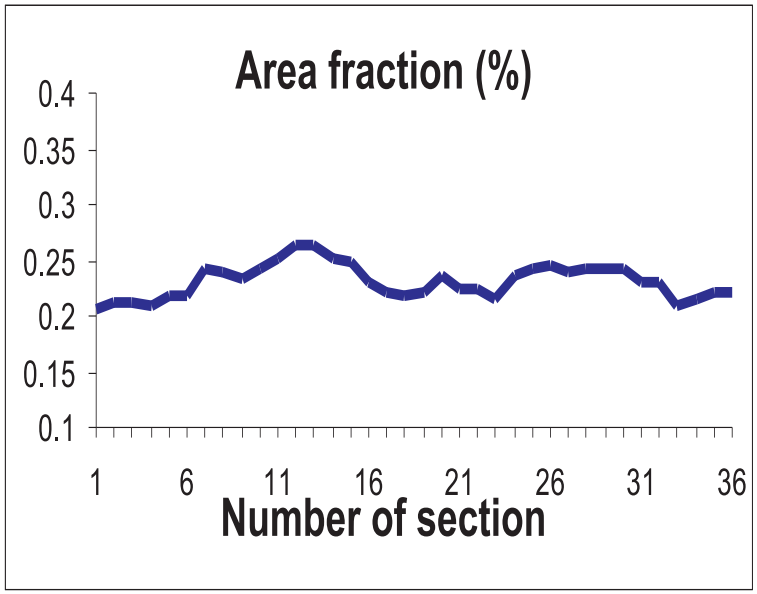

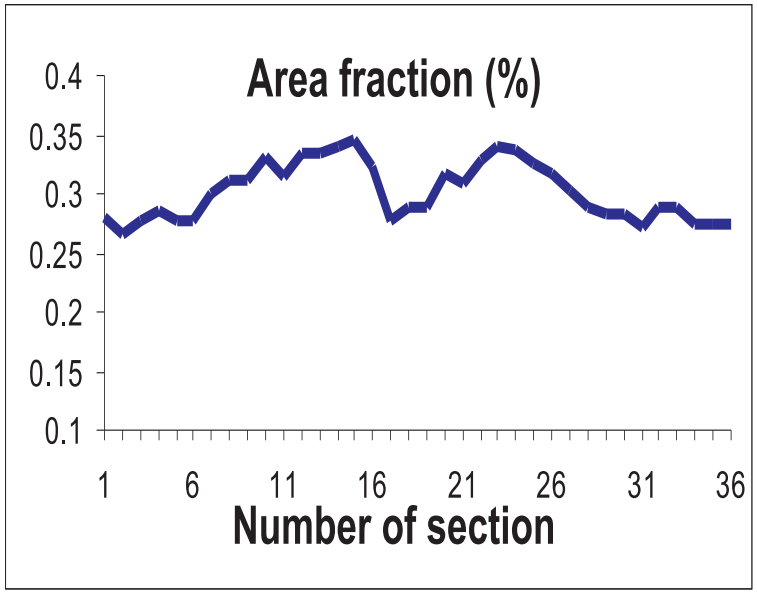

Figure: Wire-arc sprayed coating (left), plasma-sprayed coating (right)

Conclusions from comparison of two spraying techniques

General similarity in microstructure

Lamellar structures built of metallic splats

separated by oxide shells

porosity with thin cracks and irregular larger pores.

Oxidation and porosity more pronounced for plasma-sprayd coating

due to higher particle temperature (accelerates formation of oxides)

and their lower velocity (worse droplet spreading).

Corrosion resistant stainless steel coatings

worse protection in aggressive environment

Visualization of 3D phases

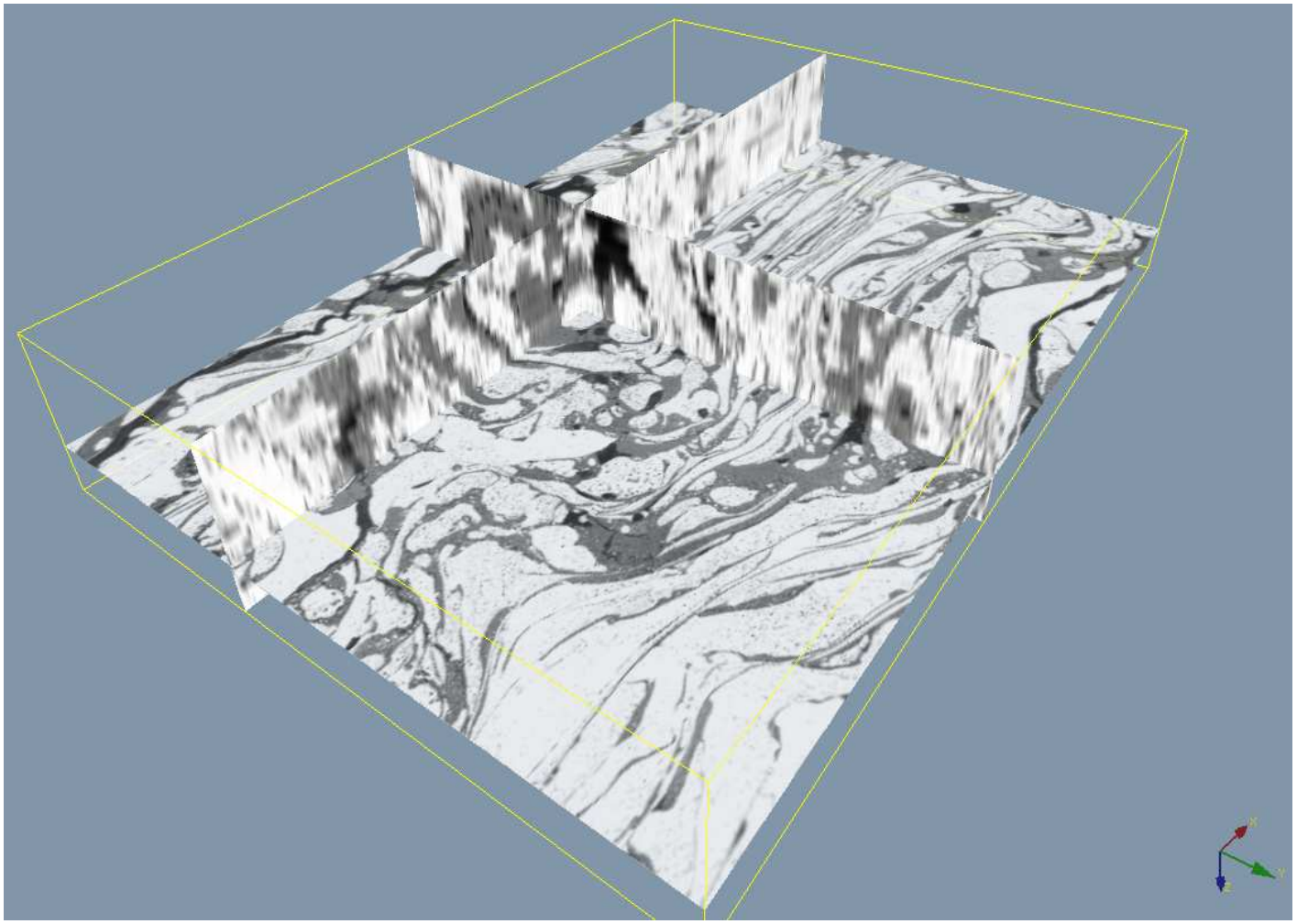

Figure: Pores and oxides in plasma-sprayed coating, using software Voxler

Visualization of 3D phases

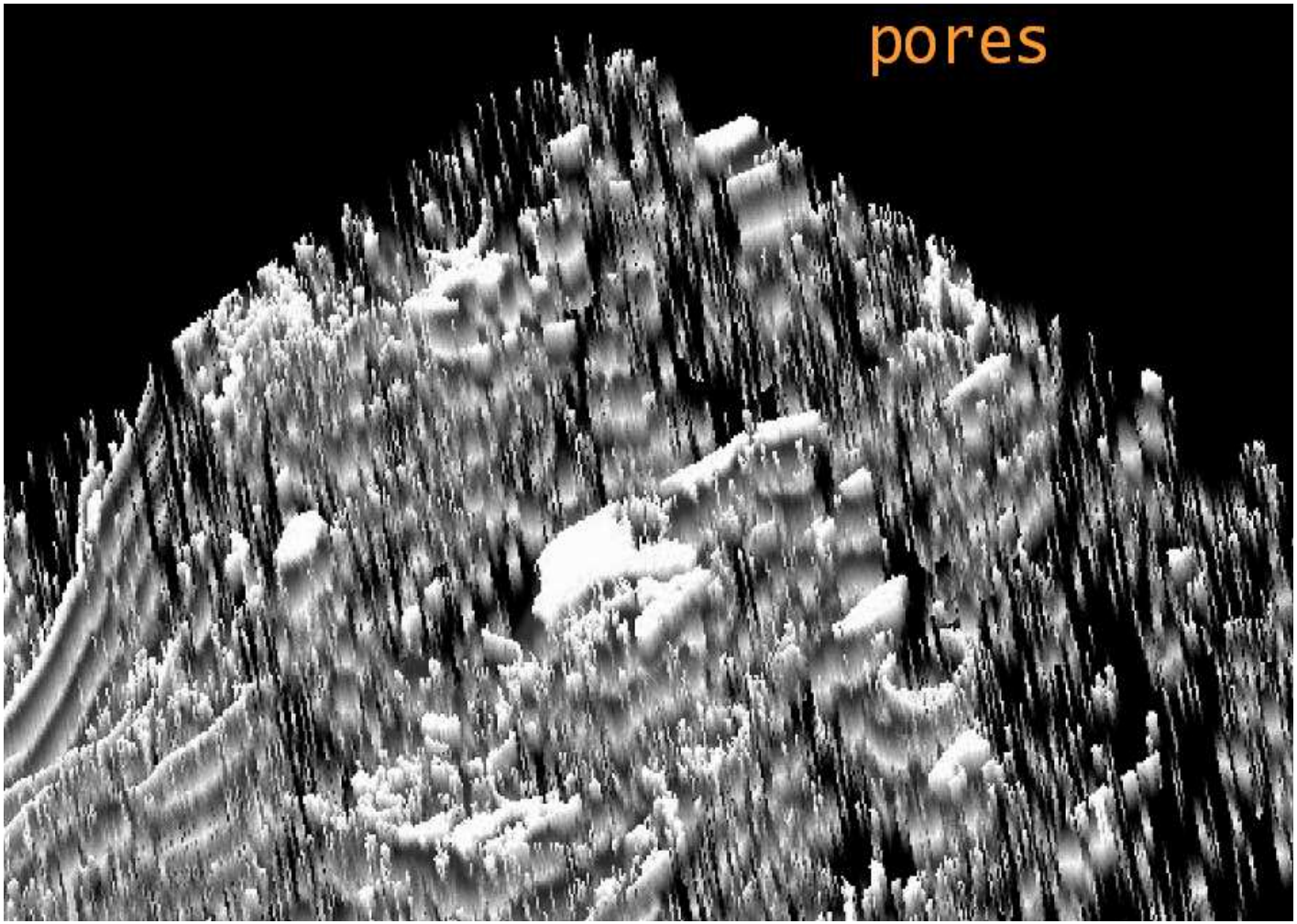

Figure: Pores in plasma-sprayed coating, using software Voxblast

Animations, anaglyphs - software Amira

References

[1] P. Ctibor, P. Hofmann, P. Chraska, R. Lechnerova, V. Benes: 3D visualization of thermally sprayed microstructure. In: Thermal Spray 2007: Global Coating Solutions. Ed. by B.R. Marple et al., ASM International, USA (2007), 878–883.

[2] P. Ctibor, R. Lechnerova, V. Benes: Quantitative analysis of pores of two types in a plasma-sprayed coating. Materials Characterization 56 (2006), 297–304.

[3] A. Kulkarni, A. Goland, H. Herman, A. Allen, J. Ilavsky, G. Long, F. De Carlo: Advanced microstructural characterization of plasma-sprayed zirconia coatings over extended length scales. J. Thermal Spray Technology, 14, 2 (2005), 239–250.

[4] A. Kulkarni, S. Sampath, A. Goland, H. Herman, B. Dowd: Computer microtomography studies to characterize microstructure-property correlations in thermal spray alumina deposits. Scripta Materialia 43 (2000), 471–476.

[5] J. Ilavsky, G. Long, A. Allen, H. Herman, C. Berndt: Use of small-angle neutron scattering for the characterization of anisotropic structures produced by thermal-spraying. Ceramics 3 (1998), 81–88.

Announcement

10th European Congress for Stereology and Image Analysis

June 22-26, 2009, Milano, Italy

www.ecs10.unimi.it